J. Plasma Phys. (2021), *vol.* 87, 905870218
Published by Cambridge University Press
doi:10.1017/S0022377821000167

How Alfvén waves energize the solar wind: heat versus work

Jean C. Perez [1],†, **Benjamin D. G. Chandran** [2], **Kristopher G. Klein** [3] and **Mihailo M. Martinović** [3,4]

[1]Department of Aerospace, Physics and Space Sciences, Florida Institute of Technology, Melbourne, FL, 32901, USA

[2]Department of Physics and Astronomy, University of New Hampshire, Durham, NH, 03824, USA

[3]Lunar and Planetary Laboratory, University of Arizona, Tucson, AZ, 85721, USA

[4]Laboratoire d'Etudes Spatiales et d'Instrumentation en Astrophysique, Observatoire de Paris, Meudon, France

(Received 16 March 2020; revised 27 January 2021; accepted 3 February 2021)

A growing body of evidence suggests that the solar wind is powered to a large extent by an Alfvén-wave (AW) energy flux. AWs energize the solar wind via two mechanisms: heating and work. We use high-resolution direct numerical simulations of reflection-driven AW turbulence (RDAWT) in a fast-solar-wind stream emanating from a coronal hole to investigate both mechanisms. In particular, we compute the fraction of the AW power at the coronal base ($P_{\rm AWb}$) that is transferred to solar-wind particles via heating between the coronal base and heliocentric distance r, which we denote by $\chi_H(r)$, and the fraction that is transferred via work, which we denote by $\chi_W(r)$. We find that $\chi_W(r_A)$ ranges from 0.15 to 0.3, where r_A is the Alfvén critical point. This value is small compared with one because the Alfvén speed v_A exceeds the outflow velocity U at $r < r_A$, so the AWs race through the plasma without doing much work. At $r > r_A$, where $v_A < U$, the AWs are in an approximate sense 'stuck to the plasma', which helps them do pressure work as the plasma expands. However, much of the AW power has dissipated by the time the AWs reach $r = r_A$, so the total rate at which AWs do work on the plasma at $r > r_A$ is a modest fraction of $P_{\rm AWb}$. We find that heating is more effective than work at $r < r_A$, with $\chi_H(r_A)$ ranging from 0.5 to 0.7. The reason that $\chi_H \geq 0.5$ in our simulations is that an appreciable fraction of the local AW power dissipates within each Alfvén-speed scale height in RDAWT, and there are a few Alfvén-speed scale heights between the coronal base and r_A. A given amount of heating produces more magnetic moment in regions of weaker magnetic field. Thus, paradoxically, the average proton magnetic moment increases robustly with increasing r at $r > r_A$, even though the total rate at which AW energy is transferred to particles at $r > r_A$ is a small fraction of $P_{\rm AWb}$.

Key words: astrophysical plasmas, space plasma physics, plasma nonlinear phenomena

1. Introduction

Following Parker's (1958) prediction that the Sun emits a supersonic wind, a number of studies attempted to model the solar wind as a spherically symmetric outflow powered

† Email address for correspondence: jcperez@fit.edu

by the outward conduction of heat from a hot coronal base (e.g. Parker 1965; Hartle & Sturrock 1968; Durney 1972; Roberts & Soward 1972). Although these studies obtained supersonic wind solutions, they were unable to reproduce the large outflow velocities measured in the fast solar wind near Earth (700–800 $\mathrm{km\,s^{-1}}$), and they did not explain the origin of the high coronal temperatures ($\sim 10^6$ K) upon which the models were based.

These shortcomings led a number of authors to conjecture that the solar wind is powered to a large extent by an energy flux carried by waves. Several observations support this idea, including *in situ* measurements of large-amplitude, outward-propagating Alfvén waves (AWs) in the interplanetary medium (e.g. Belcher & Davis 1971; Tu & Marsch 1995; Bruno & Carbone 2013) and remote observations of AW-like motions in the low corona that carry an energy flux sufficient to power the solar wind (De Pontieu *et al.* 2007).

These observations have stimulated numerous theoretical investigations of how AWs might heat and accelerate the solar wind (see, e.g., Hansteen & Velli 2012, and references therein). In many of these models, a substantial fraction of the Sun's AW energy flux is transferred to solar-wind particles by some form of dissipation. Because photospheric motions primarily launch large-wavelength AWs, and because large-wavelength AWs are virtually dissipationless, the AWs are unable to transfer their energy to the plasma near the Sun unless they become turbulent. Turbulence dramatically enhances the rate of AW dissipation because it causes AW energy to cascade from large wavelengths to small wavelengths where dissipation is rapid. One of the dominant nonlinearities that gives rise to AW turbulence is the interaction between counter-propagating AWs (Iroshnikov 1963; Kraichnan 1965). Because the Sun launches only outward-propagating waves, solar-wind models that invoke this nonlinearity require some source of inward-propagating AWs. One such source is AW reflection arising from the radial variation in the Alfvén speed (Heinemann & Olbert 1980; Velli 1993; Hollweg & Isenberg 2007). Direct numerical simulations of reflection-driven AW turbulence (RDAWT) in a fast-solar-wind stream emanating from a coronal hole (Perez & Chandran 2013; van Ballegooijen & Asgari-Targhi 2016, 2017; Chandran & Perez 2019) have shown that AW turbulence initiated by wave reflections can drive a vigorous turbulent cascade. The turbulent dissipation rates in the simulations of Perez & Chandran (2013) and Chandran & Perez (2019) are consistent with the turbulent heating rates in solar-wind models that rely on RDAWT, which have proven quite successful at explaining solar-wind observations (Cranmer, van Ballegooijen & Edgar 2007; Verdini *et al.* 2010; Chandran *et al.* 2011; van der Holst *et al.* 2014; Usmanov, Goldstein & Matthaeus 2014). (We note that there are a number of alternative approaches to incorporating AWs into solar-wind models; see, e.g., Suzuki (2006); Suzuki & Inutsuka (2006), Ofman (2010) and Shoda *et al.* (2019).)

In addition to solar-wind heating via the cascade and dissipation of AW energy, AWs energize the solar wind through the work done by the AW pressure force, which directly accelerates plasma away from the Sun (e.g. Hollweg 1973; Wang 1993). The relative importance of AW heating and AW work, however, is not well understood. Our goal in this paper is to use direct numerical simulations of RDAWT to determine the fraction of the AW power that is transferred to the solar wind via turbulent dissipation between the coronal base and radius r, denoted by $\chi_H(r)$, and the fraction that is transferred via work, denoted by $\chi_W(r)$.[1]

In § 2, we present the mathematical framework that we use to address this problem and derive mathematical expressions for $\chi_H(r)$ and $\chi_W(r)$. In § 3 we compute $\chi_H(r)$ and

[1]It is worth noting that the thermal energy generated by AW dissipation is later converted into bulk-flow kinetic energy as the solar wind expands. That process, however, does not concern us here. Our focus is to compare the work done by AWs with the heating that results from AW dissipation.

$\chi_W(r)$ in high-resolution numerical simulations of RDAWT with fixed, observationally constrained, model radial profiles for the plasma density, solar-wind outflow velocity, and background magnetic-field strength. We compare our numerical results with the values of $\chi_H(r)$ and $\chi_W(r)$ that result from a previously published analytic model of RDAWT (Chandran & Hollweg 2009). We also investigate the radial evolution of the average proton magnetic moment $k_B T_{\perp p}(r)/B(r)$ when RDAWT is the dominant proton heating mechanism, where $T_{\perp p}$ is the perpendicular proton temperature, k_B is the Boltzmann constant, and B is the magnetic-field strength.

2. Energization of the solar wind by AW turbulence

We consider turbulent fluctuations within a narrow magnetic flux tube of cross-sectional area $a(r) \ll r^2$, where r is heliocentric distance. We neglect solar rotation and take this flux tube to be centred on a radial magnetic-field line. We take the density ρ, solar-wind outflow velocity $\boldsymbol{U}$, and background magnetic field $\boldsymbol{B}_0$ to be fixed functions of r,

$$\rho = \rho(r), \quad \boldsymbol{U} = U(r)\hat{\boldsymbol{b}}, \quad \boldsymbol{B}_0 = B_0(r)\hat{\boldsymbol{b}}, \tag{2.1a–c}$$

where $\hat{\boldsymbol{b}} \equiv \boldsymbol{B}_0/B_0$. Magnetic-flux conservation implies that

$$a(r) = \frac{B_\odot}{B_0(r)} a_\odot, \tag{2.2}$$

where $a_\odot$ and $B_\odot$ are the values of $a(r)$ and $B(r)$ at the coronal base, located at $r \simeq R_\odot$, where $R_\odot$ is the solar radius. We allow for super-radial expansion of the magnetic field, but assume that a/r^2 is small enough that $\hat{\boldsymbol{b}}$ is nearly radial and $r - R_\odot$ is approximately equal to the distance from the coronal base measured along the magnetic field. We also assume that the fluctuations in the velocity and magnetic field, denoted by $\delta\boldsymbol{v}$ and $\delta\boldsymbol{B}$, are orthogonal to $\boldsymbol{B}_0$, that $\delta\boldsymbol{v}$ is divergence-free and that density fluctuations are negligibly small.

Given these simplifying assumptions, the fluctuations satisfy the equations (see, e.g., Cranmer & van Ballegooijen 2005; Verdini & Velli 2007; Chandran & Hollweg 2009)

$$\frac{\partial z^\pm}{\partial t} + (U \pm v_A)\frac{\partial z^\pm}{\partial r} + (U \mp v_A)\left(\frac{1}{4H_\rho} z^\pm - \frac{1}{2H_A} z^\mp\right) = -\left(z^\mp \cdot \nabla z^\pm - \frac{\nabla P}{\rho}\right) + \boldsymbol{D}^\pm, \tag{2.3}$$

where $z^\pm = \delta\boldsymbol{v} \mp \delta\boldsymbol{b}$ are the Elsasser variables, $\delta\boldsymbol{v}$ is the fluctuating velocity, $\delta\boldsymbol{b} = \delta\boldsymbol{B}/\sqrt{4\pi\rho}$ is the fluctuating Alfvén velocity, $v_A = B_0/\sqrt{4\pi\rho}$ is the Alfvén speed, $P = p + B^2/8\pi$ is the combined plasma and magnetic pressure, $\boldsymbol{D}^\pm$ is a dissipation term that accounts for viscosity and resistivity (or possibly hyper-viscosity and hyper-resistivity in some numerical models), and

$$\frac{1}{H_\rho} \equiv -\frac{1}{\rho}\frac{\mathrm{d}\rho}{\mathrm{d}r}, \quad \frac{1}{H_B} \equiv -\frac{1}{B_0}\frac{\mathrm{d}B_0}{\mathrm{d}r}, \quad \text{and} \quad \frac{1}{H_A} \equiv \frac{1}{v_A}\frac{\mathrm{d}v_A}{\mathrm{d}r} = \frac{1}{2H_\rho} - \frac{1}{H_B} \tag{2.4a–c}$$

are characteristic length scales of ρ, B_0 and v_A along the magnetic field, respectively. Our definition of Elsasser variables with the '$\mp$' sign convention implies that z^+ (z^-) represents AW fluctuations propagating parallel (anti-parallel) to $\boldsymbol{B}_0$ in the local plasma frame. For concreteness, we take $\boldsymbol{B}_0$ to point radially outward from the Sun so that z^+ (z^-) represents AW fluctuations that propagate anti-Sunward (Sunward) in the plasma frame. Equations (2.3) can be also seen as an inhomogeneous version of the reduced magnetohydrodynamics

(RMHD) model (Kadomtsev & Pogutse 1974; Strauss 1976) with an important new piece of physics, namely the linear coupling between z^+ and z^- fluctuations that is responsible for the non-WKB[2] reflection of AWs resulting from the spatial variation of v_A.

2.1. *Solar wind energization: how the AW power decreases with r*

The background flow and turbulent fluctuations satisfy a total-energy conservation relation, which in steady state takes the form (Chandran *et al.* 2015)

$$\boldsymbol{\nabla}\cdot[(F_{\rm flow}+F_{\rm turb})\hat{\boldsymbol{b}}]=0, \tag{2.5}$$

where

$$F_{\rm flow}=\frac{\rho U^3}{2}+\frac{\gamma U p}{\gamma-1}-\frac{GM_\odot\rho U}{r}+q_r \tag{2.6}$$

is the enthalpy flux of the background plasma, G is the universal gravitational constant, $M_\odot$ is the mass of the Sun, γ is the ratio of specific heats, q_r is the radial component of the heat flux,

$$F_{\rm turb}(r)=F^+(r)+F^-(r)+U(r)p_w(r) \tag{2.7}$$

is the enthalpy flux of the fluctuations,

$$F^\pm(r)\equiv[U(r)\pm v_A(r)]\,\mathcal{E}^\pm(r) \tag{2.8}$$

is the energy flux of the Elsasser field $z^\pm$,

$$\mathcal{E}^\pm(r)\equiv\left\langle\tfrac{1}{4}\rho|z^\pm|^2\right\rangle=\tfrac{1}{4}\rho(r)[z^\pm_{\rm rms}(r)]^2 \tag{2.9}$$

is the average energy density of Elsasser field $z^\pm$, $\langle\cdots\rangle$ denotes a statistical ensemble average,[3] and rms denotes the root-mean-square (r.m.s.) value,

$$p_w(r)=\frac{1}{2}[\mathcal{E}^+(r)+\mathcal{E}^-(r)-\mathcal{E}_R(r)]=\frac{\delta B^2_{\rm rms}(r)}{8\pi} \tag{2.10}$$

is the magnetic pressure of the fluctuations and

$$\mathcal{E}_R(r)\equiv\left\langle\frac{1}{2}\rho\boldsymbol{z}^+\cdot\boldsymbol{z}^-\right\rangle=\frac{1}{2}\rho(r)\left[\delta v^2_{\rm rms}(r)-\frac{\delta B^2_{\rm rms}(r)}{4\pi\rho(r)}\right] \tag{2.11}$$

is the average residual energy density.

Upon taking the dot product of (2.3) with $\rho\boldsymbol{z}^\pm/2$, performing an ensemble average, and summing the $+$ and $-$ versions of the equation, we obtain a separate equation describing the evolution of the fluctuation energy in steady state,

$$\boldsymbol{\nabla}\cdot[(F^+{+}F^-)\hat{\boldsymbol{b}}]=-p_w\boldsymbol{\nabla}\cdot(\hat{\boldsymbol{b}}U)-\sigma U\mathcal{E}_R-Q, \tag{2.12}$$

where

$$Q=\langle\tfrac{1}{2}\rho(\boldsymbol{z}^+\cdot\boldsymbol{D}^+{+}\boldsymbol{z}^-\cdot\boldsymbol{D}^-)\rangle \tag{2.13}$$

is the average turbulent heating rate, and $\sigma=\boldsymbol{\nabla}\cdot\hat{\boldsymbol{b}}=1/H_B$. When $\mathcal{E}_R\to0$, $\mathcal{E}^-/\mathcal{E}^+\to0$ and $Q\to0$, equation (2.12) reduces to equation (42) of Dewar (1970), which is equivalent

[2]WKB stands for the well known Wentzel–Kramers–Brillouin approximation for finding solutions of linear wave equations with variable coefficients.

[3]Note that because we assume the system is statistically stationary and homogeneous at each heliocentric distance, ensemble-averaged quantities are only a function of r.

to the statement that the action of outward-propagating AWs is conserved. Combining (2.7) and (2.12), we obtain the relation

$$\boldsymbol{\nabla}\cdot(F_{\rm turb}\hat{\boldsymbol{b}}) = \frac{1}{a(r)}\frac{{\rm d}P_{\rm AW}}{{\rm d}r} = -\sigma U\mathcal{E}_R + U\frac{{\rm d}p_w}{{\rm d}r} - Q, \tag{2.14}$$

where

$$P_{\rm AW}(r) = a(r)F_{\rm turb}(r) \tag{2.15}$$

is the AW power. For the solar wind case, in which $\mathcal{E}^+ > \mathcal{E}^-$ and $P_{\rm AW} > 0$, equation (2.14) describes how the AW power decreases with increasing r. Equation (2.5) implies that $P_{\rm AW}(r) + P_{\rm flow}(r)$ is independent of r, where $P_{\rm flow} = a(r)F_{\rm flow}(r)$ is the power carried by the outflowing background plasma. Thus, as $P_{\rm AW}$ decreases, $P_{\rm flow}$ increases and energy is transferred from the AW fluctuations to the background without loss.

By multiplying (2.14) by $a(r)$ and integrating from the coronal base at $r = r_b$ out to radius r, we obtain

$$P_{\rm AW}(r) - P_{\rm AWb} = \int_{r_b}^{r} a(r')U(r')\left[\frac{\rm d}{{\rm d}r'}p_w(r') - \sigma(r')\mathcal{E}_R(r')\right]{\rm d}r' - \int_{r_b}^{r} a(r')Q(r')\,{\rm d}r', \tag{2.16}$$

where the 'b' subscript indicates that the subscripted quantity ($P_{\rm AW}$ in this case) is evaluated at $r = r_b$. The first term inside the first integral of (2.16) is the negative of the radial component of the pressure force on a plasma parcel of thickness ${\rm d}r$, $-a({\rm d}p_w/{\rm d}r)\,{\rm d}r$, multiplied by the radial velocity U, which has the familiar force-times-velocity form of mechanical power and represents the rate at which $P_{\rm AW}$ decreases with increasing radius due to the work done by AWs on the flow. When residual energy $\mathcal{E}_R$ is negative, which has been shown to result from the nonlinear interaction of counter-propagating AWs (Müller & Grappin 2005; Boldyrev *et al.* 2011; Wang, Boldyrev & Perez 2011), the second term in the first integral results in a small reduction of the net work done by the AW pressure. However, positive residual energy is possible in RDAWT when linear terms responsible for non-WKB reflection dominate nonlinear terms and when ${\rm d}v_A/{\rm d}r > 0$, in which case the residual energy will be responsible for a slight increase in the net work done by the AW pressure. The second integral in (2.16) represents the rate of decrease in $P_{\rm AW}$ due to dissipation and turbulent heating. We rewrite (2.16) as

$$P_{\rm AW}(r) - P_{\rm AWb} = -H(r) - W(r), \tag{2.17}$$

where

$$H(r) = \int_{\rm r_b}^{r} a(r')Q(r')\,{\rm d}r', \tag{2.18}$$

$$W(r) = -\int_{\rm r_b}^{r} a(r')U(r')\left[\frac{\rm d}{{\rm d}r'}p_w(r') - \sigma(r')\mathcal{E}_R(r')\right]{\rm d}r' \tag{2.19}$$

are the rates at which energy is transferred from the fluctuations to the background flow in the radial interval (r_b, r) via heat and work, respectively. We then divide (2.17) by $-P_{\rm AWb}$

and rearrange terms to obtain

$$\frac{P_{\rm AW}}{P_{\rm AWb}} + \chi_H + \chi_W = 1, \tag{2.20}$$

where

$$\chi_H(r) = \frac{H(r)}{P_{\rm AWb}}, \quad \chi_W(r) = \frac{W(r)}{P_{\rm AWb}}. \tag{2.21a,b}$$

The first term on the left-hand side of (2.20) is the fraction of the coronal-base AW power $P_{\rm AWb}$ that survives to radius r. The second term $\chi_H(r)$ is the fraction of $P_{\rm AWb}$ that is transferred to solar-wind particles via dissipation and heating between r_b and r. The third term χ_W is the fraction of $P_{\rm AWb}$ that is transferred to solar-wind particles via work in the radial interval (r_b, r).

3. Heat and work fractions of AW power transferred by RDAWT

In this section, we compute the rates at which AW fluctuation energy is transferred to the background solar wind via heating and work in direct numerical simulations of RDAWT. We also compute these same rates using an approximate analytic model of RDAWT. The numerical simulations were carried out using the pseudo-spectral Chebyshev–Fourier REFLECT code (Perez & Chandran 2013), which solves (2.3) in the narrow-fluxtube geometry described in the previous section.

3.1. *Numerical simulations*

We consider the three simulations labelled Run 1, Run 2 and Run 3 in the work of Chandran & Perez (2019), in which

$$\rho(r) = m_p n(r), \tag{3.1}$$

$$n(r) = (3.23 \times 10^8 x^{-15.6} + 2.51 \times 10^6 x^{-3.76} + 1.85 \times 10^5 x^{-2})\ {\rm cm}^{-3}, \tag{3.2}$$

$$B_0(r) = [1.5(f_{\rm max} - 1)x^{-6} + 1.5x^{-2}]\ {\rm G}, \tag{3.3}$$

$$U(r) = 9.25 \times 10^{12} \frac{B_{\rm G}}{\tilde{n}}\ {\rm cm\,s^{-1}}, \tag{3.4}$$

where n is the proton number density, m_p is the proton mass, $x = r/R_\odot$, $f_{\rm max}$ is the super-radial expansion factor (Kopp & Holzer 1976), which we set equal to 9, $B_{\rm G}$ is $B_0(r)$ in Gauss and $\tilde{n}$ is $n(r)$ in units of ${\rm cm}^{-3}$. In all three runs, the simulation domain consists of a narrow magnetic flux tube with a square cross section of area $[L_\perp(r)]^2$ extending from the photosphere ($r = R_\odot$) out to approximately $r = 21R_\odot$. The Alfvén critical point in these simulations, defined as the heliocentric radius at which the local Alfvén speed equals the solar wind speed, is located at $r = r_A \simeq 11.1R_\odot$ (for a list of relevant heliocentric radii see table 2). Equation (2.2) implies that

$$L_\perp(r) = L_{\perp,b}\sqrt{\frac{a(r)}{a_\odot}} = L_{\perp,b}\sqrt{\frac{B_\odot}{B(r)}}, \tag{3.5}$$

where $L_{\perp,b}$ is the width of the simulation domain at the coronal base.

AWs are injected into the solar corona by imposing a broad spectrum of z^+ fluctuations at the coronal base, located at $r = 1.0026R_\odot$ in our simulations (approximately 1800 km above the photosphere), which then propagate outwards and generate reflected

Parameter		Run 1	Run 2	Run 3
$\tau^+_{c,p}$	.....	3.3 min	9.6 min	9.3 min
$\tau^+_{c,b}$	.....	0.3 min	0.3 min	1.6 min
$L_{\perp,b}$	.....	4100 km	4100 km	16 000 km
$z^+_{\mathrm{rms},b}$	.....	60 km s^{-1}	55 km s^{-1}	40 km s^{-1}
$\delta v_{\mathrm{rms},b}$	.....	31 km s^{-1}	28 km s^{-1}	21 km s^{-1}

TABLE 1. Relevant simulation parameters. At the photosphere: $\tau^+_{c,p}$ is the correlation time of velocity fluctuations imposed at $r = R_\odot$. At the coronal base: $\tau^+_{c,p}$ is the correlation time of outward-propagating AWs (z^+), $L_{\perp,b}$ is the perpendicular box length, z^+_{rms} is the r.m.s. amplitude of AWs injected at the base, and $v_{\mathrm{rms,b}}$ is the bulk velocity r.m.s.

(inward-propagating) waves that drive the turbulent cascade. A strong-turbulence spectrum at the coronal base is achieved by adding a model chromosphere just below the coronal base, with a sharp transition region modelled as a discontinuity of the background profiles. Although the model chromosphere ignores important effects, such as compressibility, it allows us to generate a strong turbulence spectrum of fluctuations driven by reflections from strong inhomogeneities in the chromosphere and the sharp transition region.

The three simulations, which are described in greater detail in Chandran & Perez (2019) and a subsequent publication, differ only in the properties of the photospheric velocity field imposed at the inner boundary, namely, the r.m.s. amplitudes of the velocity fluctuations, the correlation lengths and the correlation times. These parameters, listed in table 1, are chosen to investigate how the turbulence properties at each r depend on the properties of the fluctuations at the coronal base within observational constraints. For instance, the width of the simulation domain at the coronal base, $L_{\perp,b}$, is chosen to allow for characteristic correlation lengths of AWs launched at the base to be consistent with observational estimates between 10^3 km to 10^4 km (Dmitruk *et al.* 2002; Cranmer *et al.* 2007; Verdini & Velli 2007; Hollweg, Cranmer & Chandran 2010; Verdini *et al.* 2012; van Ballegooijen & Asgari-Targhi 2016, 2017). Similarly, photospheric velocity driving with amplitude $\delta v_{\mathrm{rms}} \simeq 1.3$ km s^{-1} and characteristic times between 3 and 10 min leads to $\delta v_{\mathrm{rms},b}$ values between 20 and 30 km s^{-1} with correlation times between 0.3 and 1.6 min.

3.2. *Analytic model of RDAWT*

Chandran & Hollweg (2009) (hereafter CH09) developed an analytic model of RDAWT based on (2.3) but with the additional assumption that

$$z^+_{\mathrm{rms}} \gg z^-_{\mathrm{rms}}, \tag{3.6}$$

which implies that

$$\mathcal{E}^+ + \mathcal{E}^- \simeq \tfrac{1}{4}\rho (z^+_{\mathrm{rms}})^2. \tag{3.7}$$

Given (3.6), CH09 estimated the turbulent heating rate to be

$$Q = \frac{\rho z^-_{\mathrm{rms}} (z^+_{\mathrm{rms}})^2}{4\lambda_\perp}, \tag{3.8}$$

where $\lambda_\perp$ is the correlation length of the turbulence measured perpendicular to $\boldsymbol{B}_0$. Following Dmitruk *et al.* (2002), CH09 estimated z^-_{rms} by balancing the rate at which z^- is

produced by non-WKB reflection against the rate at which z^- cascades to small scales and dissipates in the small-$\lambda_\perp$ limit, obtaining

$$z^-_{\rm rms}(r) = \frac{\lambda_\perp (U + v_A)}{v_A} \left| \frac{{\rm d}v_A}{{\rm d}r} \right|, \tag{3.9}$$

which is independent of $z^+_{\rm rms}$, because the source and sink terms for z^- are both proportional to $z^+_{\rm rms}$. CH09 then used (3.6) and (3.9) to solve (2.14), obtaining

$$[z^+_{\rm rms}(r)]^2 = (z^+_{{\rm rms},b})^2 \frac{\eta^{1/2}}{\eta_b^{1/2}} \left(\frac{1 + \eta_b^{1/2}}{1 + \eta^{1/2}} \right)^2 h(r), \tag{3.10}$$

where

$$\eta(r) = \frac{\rho(r)}{\rho(r_A)}, \tag{3.11}$$

$$h(r) = \begin{cases} v_{\rm Ab}/v_A(r), & \text{if } r_b < r < r_m, \\ v_{\rm Ab} v_A(r)/v^2_{\rm Am}, & \text{if } r > r_m, \end{cases} \tag{3.12}$$

and $v_{\rm Am}$ is the maximum Alfvén speed in the corona, which occurs at $r = r_m$. (CH09 assumed that v_A increased monotonically with increasing r between r_b and r_m, and then decreased monotonically with increasing r at $r > r_m$.) The CH09 model reduces to the model of Dmitruk *et al.* (2002) in the limit $U \to 0$.

Mass and magnetic-flux conservation imply that

$$\frac{\rho U}{B_0} = \text{constant}. \tag{3.13}$$

This equation and the condition that $U(r_A) = v_A(r_A)$ imply that

$$v_A = \eta^{1/2} U. \tag{3.14}$$

The density at the coronal base exceeds the density at the Alfvén critical point by a large factor ($\simeq 10^5$ in the fast-solar-wind model of Chandran *et al.* 2011). Thus,

$$1 + \eta_b^{1/2} \simeq \eta_b^{1/2}. \tag{3.15}$$

Given (2.15), (3.6), (3.14) and (3.15),

$$P_{\rm AWb} \simeq \tfrac{1}{4} a_b v_{\rm Ab} \rho_b (z^+_{{\rm rms},b})^2. \tag{3.16}$$

Upon substituting (3.8), (3.9), (3.10) and (3.16) into (2.18) and (2.21*a*,*b*), we obtain

$$\chi_H(r) = \int_{r_b}^{r} \left[\frac{\eta(r')^{1/2}}{1 + \eta(r')^{1/2}} \right] \frac{1}{v_A(r')} \left| \frac{{\rm d}v_A(r')}{{\rm d}r'} \right| h(r')\, {\rm d}r'. \tag{3.17}$$

Equations (2.15), (3.10) and (3.15) imply that

$$\frac{P_{\rm AW}}{P_{\rm AWb}} = \left(\frac{3}{2} + \eta^{1/2} \right) \eta^{1/2} (1 + \eta^{1/2})^{-2} h(r). \tag{3.18}$$

It then follows from (2.20) and (3.18) that

$$\chi_W = 1 - \chi_H - \left(\tfrac{3}{2} + \eta^{1/2} \right) \eta^{1/2} (1 + \eta^{1/2})^{-2} h(r). \tag{3.19}$$

Quantity		Meaning	Numerical value in CH09
r_b	.....	Radius of coronal base	$1.0026R_s$
r_m	.....	Radius of Alfvén-speed maximum	$1.72R_s$
r_A	.....	Radius of Alfvén critical point	$11.1R_s$
$v_{\rm Ab}$	.....	Alfvén speed at $r = r_b$	906 km s^{-1}
$v_{\rm Am}$	.....	Alfvén speed at $r = r_m$	2430 km s^{-1}
$v_{\rm Aa}$	.....	Alfvén speed at $r = r_A$	626 km s^{-1}
U(1 au)	.....	Solar-wind outflow velocity at Earth	750 km s^{-1}

TABLE 2. Glossary of relevant quantities and their numerical values.

3.3. *The fractions of the AW power that are converted into heat and work*

Figure 1 shows the fractions χ_H, χ_W and $P_{\rm AW}/P_{\rm AWb}$ for Run 1, Run 2 and Run 3, as well as the corresponding fractions calculated from the analytic model described in the previous section, using (3.2), (3.3), (3.4), (3.17), (3.18), (3.19) and the numerical values of relevant parameters listed in table 2. In the simulations, the heating fractions are calculated using (2.9), (2.10), (2.11), (2.13), (2.18) and (2.19). Assuming ergodicity in space and time at each radius, ensemble averages in (2.9), (2.11) and (2.13) are computed using a combined average over time (during the simulation's steady state) and over the cross-sectional area of the fluxtube. More precisely, ensemble averages of any quantity $f = f(\boldsymbol{x}, t)$ in the simulations are computed as

$$\langle f \rangle \equiv \frac{1}{T}\int_0^T \left(\frac{1}{a}\int_S f \,{\rm d}a\right) {\rm d}t, \tag{3.20}$$

where S is the cross-sectional surface of the fluxtube at each radius.

The reason that $\chi_H(r_A)$ is greater than 0.5 in the simulations is that a moderate fraction of the remaining AW energy flux dissipates each time the outward-propagating AWs pass through one Alfvén-speed scale height (Dmitruk *et al.* 2002; Chandran & Hollweg 2009), and there are a few Alfvén-speed scale heights between $r = r_b$ and $r = r_A$. On the other hand, the work fraction $\chi_W \lesssim 0.3$ is significantly smaller because $v_A > U$ at $r < r_A$, and thus AWs at $r < r_A$ are in an approximate sense speeding through a quasi-stationary background without doing much work. In contrast, at $r > r_A$, $v_A < U$ and the AWs can be thought of as being 'stuck to the plasma', which enhances the rate at which the fluctuations do work and causes work to become somewhat more efficient than heating. For example, $\chi_W(21R_\odot) - \chi_W(r_A)$ equals 0.05, 0.027, 0.062 and 0.017 in Run 1, Run 2, Run 3 and the analytic model, respectively, whereas $\chi_H(21R_\odot) - \chi_H(r_A)$ equals 0.04, 0.026, 0.055 and 0.016 in Run 1, Run 2, Run 3 and the analytic model, respectively. Although work is slightly more efficient than heating at transferring energy from AWs to solar-wind particles between $r = r_A$ and $r = 21R_\odot$, most of the AW energy flux has dissipated by the time the AWs reach r_A, and the amount of AW power that is transferred to particles via work in this region is only a tiny fraction ($\lesssim 6\,\%$) of $P_{\rm AWb}$.

The different efficiencies of AW energy loss via work inside and outside the Alfvén critical point are in some ways analogous to the different rates at which energetic particles lose energy in the expanding solar wind in the scatter-free and scatter-dominated regimes (Ruffolo 1995). When pitch-angle scattering is weak, energetic particles race through the plasma, their energies are approximately conserved, and they do negligible work on the plasma. In contrast, when pitch-angle scattering is strong, energetic particles are

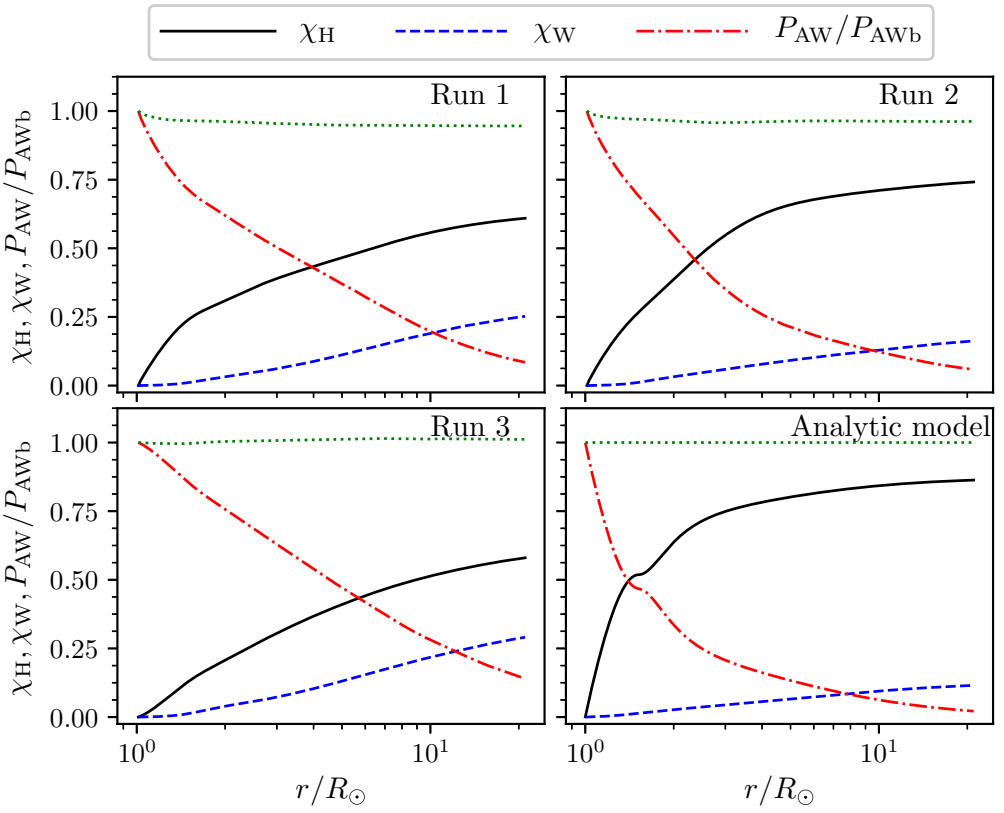

FIGURE 1. Fractions of the Sun's AW power injected at the base $\chi_H(r)$ (solid) and $\chi_W(r)$ (dashed) that are transferred to solar-wind particles via heating and work, respectively, between the coronal base and heliocentric distance r. Here P_{AW}/P_{AWb} (dashed-dotted) is the fraction of the power that remains at each heliocentric distance r. These fractions are evaluated for Run 1, Run 2 and Run 3 using the expressions in § 2.1 and for the CH09 analytic model (lower-right panel) using the expressions in § 3.2. All four panels are computed using the $n(r)$, $B_0(r)$ and $U(r)$ profiles in (3.2) through (3.4). The green dotted lines represent the sum of the three fractions, which owing to energy conservation equals one in steady state. Small deviations from one in the numerical simulations are due primarily to averaging over a finite number of realizations rather than a full ensemble representing a true statistical state.

'stuck to the plasma', and they lose energy through adiabatic expansion, because the scattering centers that 'collide' with the particles are rooted in the plasma and diverge from one another as the plasma expands. As the particles lose energy, they do work on the background flow.

In figure 2(*a*), we plot the ratio of Q to $|U\,\mathrm{d}p_W/\mathrm{d}r - \sigma U\mathcal{E}_R|$. These two quantities are the rates of heating and work per unit volume, which appear on the right-hand side of (2.16). This figure further illustrates the increasing relative efficiency of work beyond the Alfvén critical point, where the AWs become less mobile with respect to the plasma frame. The sharp feature in $Q/|U\,\mathrm{d}p_W/\mathrm{d}r - \sigma U\mathcal{E}_R|$ at $r = r_m = 1.72R_\odot$ in the analytic model (in which $\mathcal{E}_R$ is taken to be negligible in comparison with p_W) is an artefact of the local nature of the CH09 model, in which z^-_{rms} is determined at each r by balancing the local rate of wave reflection against the local rate at which z^- fluctuations cascade and dissipate. This local balance causes z^-_{rms} and Q to be proportional to $|\mathrm{d}v_A/\mathrm{d}r|$, which

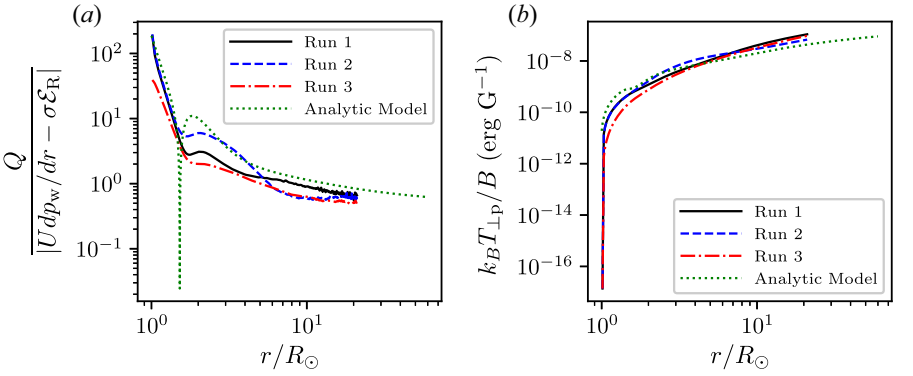

FIGURE 2. (*a*) The ratio of the heating rate Q to the rate at which AWs do work on the flow per unit volume, $|U\,\mathrm{d}p_w/\mathrm{d}r - \sigma\mathcal{E}_R|$, as a function of heliocentric distance r. Heating is much more efficient than work close to the Sun, but at $r > r_A = 11.1R_\odot$, work becomes slightly more efficient than heating. Right panel: The average proton magnetic moment, $k_BT_{\perp p}/B$, as a function of heliocentric distance r, computed using (3.8), (3.9), (3.10), (3.22), (3.2), (3.3) and (3.4), with $f_{\perp p} = 0.9$, $z^+_{\mathrm{rms,b}} = 72\ \mathrm{km\,s^{-1}}$ and $T_{\perp pb} = 10^6$ K.

vanishes at $r = r_m$. In our numerical simulations, z^- fluctuations propagate some radial distance before dissipating, and z^-_{rms} and Q remain non-zero at $r = r_m$, as seen in the Q profiles for numerical simulations shown in figure 2.

3.4. *Magnetic-moment production*

Beyond the sonic point at $r = r_s$ ($r_s \simeq 2R_\odot$ in coronal holes), the solar-wind outflow velocity exceeds the proton thermal speed v_{Tp}, and the expansion time scale r/U becomes shorter than the minimum time in which heat can conduct over a distance r, which is approximately r/v_{Tp}. Proton thermal conduction can thus be neglected to a reasonable approximation at $r > r_s$. For simplicity, in this section, we neglect proton thermal conduction at all r. We also neglect energy transfer from proton–electron collisions, as well as temperature isotropization from collisions and instabilities. The rate at which the average proton magnetic moment $k_BT_{\perp p}/B$ increases with r is then given by Sharma *et al.* (2006) and Chandran *et al.* (2011)

$$BnU\frac{\mathrm{d}}{\mathrm{d}r}\left(\frac{k_BT_{\perp p}}{B}\right) = f_{\perp p}Q, \tag{3.21}$$

where k_B is the Boltzmann constant, $T_{\perp p}$ is the perpendicular proton temperature and $f_{\perp p}(r)$ is the fraction of the heating rate that goes into perpendicular proton heating at heliocentric distance r. We approximate (3.21) by setting $B(r) = B_0(r)$. Upon dividing (3.21) by B_0nU, integrating and making use of (3.13), we obtain

$$\frac{k_BT_{\perp p}}{B_0} = \frac{k_BT_{\perp pb}}{B_{0b}} + \int_{r_b}^{r}\frac{f_{\perp p}(r')Q(r')B_{0b}}{n_bU_b[B_0(r')]^2}\,\mathrm{d}r'. \tag{3.22}$$

The form of the integrand in (3.22) shows that a given amount of heating produces more magnetic moment in regions of weaker magnetic field.

In figure 2(*b*), we plot the average magnetic moment $k_BT_{\perp p}/B$ as a function of r using (3.2), (3.3), (3.4), (3.8), (3.9), (3.10) and (3.22), with $f_{\perp p} = 0.9$, $z^+_{\mathrm{rms,b}} = 72\ \mathrm{km\,s^{-1}}$ and $T_{\perp pb} = 10^6$ K. Figures 1 and 2 show that, although only a small fraction of P_{AWb} is dissipated at $r > r_A$, $k_BT_{\perp p}/B$ rises robustly at $r > r_A$.

4. Conclusion

In this paper, we have used direct numerical simulations of RDAWT to determine $\chi_H(r)$ and $\chi_W(r)$, the fractions of the AW power at the coronal base ($P_{\rm AWb}$) that are transferred to the solar wind via heating and work between the coronal base ($r = r_b$) and radius r. Our simulations solve for the evolution of transverse, non-compressive fluctuations in a fixed background solar wind whose density, magnetic-field strength and outflow-velocity profiles are chosen to emulate a fast-solar-wind stream emanating from a coronal hole. We have found that heating from the cascade and dissipation of AW fluctuations between r_b and the Alfvén critical point r_A transfers between 50 % and 70 % of $P_{\rm AWb}$ to the solar wind, whereas work in this same region transfers between 15 % and 30 % of $P_{\rm AWb}$ to the solar wind. The variation in these numbers arises from the different photospheric boundary conditions imposed in our different numerical simulations.

The reason that $\chi_H(r_A)$ is in the range of 50–70 % is that a moderate fraction of the local AW power dissipates within each Alfvén speed scale height (Dmitruk *et al.* 2002; Chandran & Hollweg 2009), and there are a few Alfvén speed scale heights between r_b and r_A. The reason that $\chi_W(r_A)$ is small compared with one is that $v_A > U$ at $r < r_A$, so AWs in this sub-Alfvénic region are in an approximate sense speeding through a quasi-stationary background without doing much work. Work becomes relatively more efficient at transferring AW energy to the particles at $r > r_A$, where $v_A < U$ and the AWs are in an approximate sense 'stuck to the plasma'. However, because most of the Sun's AW power dissipates via heating before the AWs reach r_A, the total rate at which work transfers AW energy to the plasma at $r > r_A$ is a small fraction of $P_{\rm AWb}$. Although only a small fraction of $P_{\rm AWb}$ survives to reach r_A, the average proton magnetic moment increases robustly at $r > r_A$ (assuming that a substantial fraction of the turbulent heating rate goes into perpendicular proton heating at these radii), because heating becomes more effective at producing magnetic moment in regions of weaker magnetic field.

The accuracy of our results is limited by our neglect of compressive fluctuations, which enhance the dissipation of AW energy via 'AW phase mixing' (Heyvaerts & Priest 1983). Plasma compressibility further enhances the rate of AW dissipation via parametric decay (Galeev & Oraevskii 1963; Sagdeev & Galeev 1969; Cohen & Dewar 1974; Goldstein 1978; Spangler 1986; Hollweg 1994; Dorfman & Carter 2016; Tenerani, Velli & Hellinger 2017; Chandran 2018). Three-dimensional compressible MHD simulations of the turbulent solar wind from $r = r_b$ out to $r > r_A$, such as those carried out by Shoda *et al.* (2019), could lead to improved estimates of $\chi_H(r)$ and $\chi_W(r)$.

Acknowledgements

We thank J. Hollweg, M. Lee, B. Metzger and E. Quataert for valuable discussions. J.C.P. was supported by NSF grant AGS-1752827. B.D.G.C. was supported in part by NASA grants NNX17AI18G and 80NSSC19K0829 and NASA grant NNN06AA01C to the Parker Solar Probe FIELDS Experiment. K.G.K. was supported in part by NASA ECIP grant 80NSSC19K0912 and the Parker Solar Probe SWEAP contract NNN06AA01C. M.M. was supported in part by NASA grant 80NSSC19K1390. An award of computer time was provided by the Innovative and Novel Computational Impact on Theory and Experiment (INCITE) program. During the INCITE award period (from 2012 to 2014), this research used resources of the Argonne Leadership Computing Facility, which is a DOE Office of Science User Facility supported under Contract DE-AC02-06CH11357. This work also used high-performance computing resources of the Texas Advanced Computing Center (TACC) at the University of Texas at Austin, under project TG-ATM100031 of the

Extreme Science and Engineering Discovery Environment (XSEDE), which is supported by National Science Foundation grant number ACI-1548562.

Editor Alex Schekochihin thanks the referees for their advice in evaluating this article.

Declaration of interests

The authors report no conflicts of interest.

REFERENCES

VAN BALLEGOOIJEN, A. A. & ASGARI-TARGHI, M. 2016 Heating and acceleration of the fast solar wind by Alfvén wave turbulence. *Astrophys. J.* **821**, 106.

VAN BALLEGOOIJEN, A. A. & ASGARI-TARGHI, M. 2017 Direct and inverse cascades in the acceleration region of the fast solar wind. *Astrophys. J.* **835**, 10.

BELCHER, J. W., DAVIS, L. JR., 1971 Large-amplitude Alfvén waves in the interplanetary medium, 2. *J. Geophys. Res.* **76**, 3534–3563.

BOLDYREV, S., PEREZ, J. C., BOROVSKY, J. E. & PODESTA, J. J. 2011 Spectral scaling laws in magnetohydrodynamic turbulence simulations and in the solar wind. *Astrophys. J. Lett.* **741**, L19.

BRUNO, R. & CARBONE, V. 2013 The solar wind as a turbulence laboratory. *Living Rev. Sol. Phys.* **10** (1), 2.

CHANDRAN, B. D. G. 2018 Parametric instability, inverse cascade and the range of solar-wind turbulence. *J. Plasma Phys.* **84**, 905840106.

CHANDRAN, B. D. G., DENNIS, T. J., QUATAERT, E. & BALE, S. D. 2011 Incorporating kinetic physics into a two-fluid solar-wind model with temperature anisotropy and low-frequency Alfvén-wave turbulence. *Astrophys. J.* **743**, 197.

CHANDRAN, B. D. G. & HOLLWEG, J. V. 2009 Alfvén wave reflection and turbulent heating in the solar wind from 1 solar radius to 1 AU: an analytical treatment. *Astrophys. J.* **707**, 1659–1667.

CHANDRAN, B. D. G. & PEREZ, J. C. 2019 Reflection-driven magnetohydrodynamic turbulence in the solar atmosphere and solar wind. *J. Plasma Phys.* **85** (4), 905850409.

CHANDRAN, B. D. G., PEREZ, J. C., VERSCHAREN, D., KLEIN, K. G. & MALLET, A. 2015 On the conservation of cross helicity and wave action in solar-wind models with non-WKB Alfvén wave reflection. *Astrophys. J.* **811**, 50.

COHEN, R. H. & DEWAR, R. L. 1974 On the backscatter instability of solar wind Alfven waves. *J. Geophys. Res.* **79**, 4174–4178.

CRANMER, S. R. & VAN BALLEGOOIJEN, A. A. 2005 On the generation, propagation, and reflection of Alfvén waves from the solar photosphere to the distant heliosphere. *Astrophys. J. Suppl.* **156**, 265–293.

CRANMER, S. R., VAN BALLEGOOIJEN, A. A. & EDGAR, R. J. 2007 Self-consistent coronal heating and solar wind acceleration from anisotropic magnetohydrodynamic turbulence. *Astrophys. J. Suppl.* **171**, 520–551.

DE PONTIEU, B., MCINTOSH, S. W., CARLSSON, M., HANSTEEN, V. H., TARBELL, T. D., SCHRIJVER, C. J., TITLE, A. M., SHINE, R. A., TSUNETA, S., KATSUKAWA, Y., *et al.* 2007 Chromospheric Alfvénic waves strong enough to power the solar wind. *Science* **318**, 1574–1577.

DEWAR, R. L. 1970 Interaction between hydromagnetic waves and a time-dependent, inhomogeneous medium. *Phys. Fluids* **13**, 2710–2720.

DMITRUK, P., MATTHAEUS, W. H., MILANO, L. J., OUGHTON, S., ZANK, G. P. & MULLAN, D. J. 2002 Coronal heating distribution due to low-frequency, wave-driven turbulence. *Astrophys. J.* **575**, 571–577.

DORFMAN, S. & CARTER, T. A. 2016 Observation of an Alfvén wave parametric instability in a laboratory plasma. *Phys. Rev. Lett.* **116** (19), 195002.

DURNEY, B. R. 1972 Solar-wind properties at the earth as predicted by one-fluid models. *J. Geophys. Res.* **77**, 4042–4051.

GALEEV, A. A. & ORAEVSKII, V. N. 1963 The stability of Alfvén waves. *Sov. Phys. Dokl.* **7**, 988.

GOLDSTEIN, M. L. 1978 An instability of finite amplitude circularly polarized Alfven waves. *Astrophys. J.* **219**, 700–704.

HANSTEEN, V. H. & VELLI, M. 2012 Solar wind models from the chromosphere to 1 AU. *Space Sci. Rev.* **172** (1–4), 89–121.

HARTLE, R. E. & STURROCK, P. A. 1968 Two-fluid model of the solar wind. *Astrophys. J.* **151**, 1155.

HEINEMANN, M. & OLBERT, S. 1980 Non-WKB Alfven waves in the solar wind. *J. Geophys. Res.* **85**, 1311–1327.

HEYVAERTS, J. & PRIEST, E. R. 1983 Coronal heating by phase-mixed shear Alfven waves. *Astron. Astrophys.* **117**, 220–234.

HOLLWEG, J. V. 1973 Alfvén waves in a two-fluid model of the solar wind. *Astrophys. J.* **181**, 547–566.

HOLLWEG, J. V. 1994 Beat, modulational, and decay instabilities of a circularly polarized Alfven wave. *J. Geophys. Res.* **99**, 23.

HOLLWEG, J. V., CRANMER, S. R. & CHANDRAN, B. D. G. 2010 Coronal faraday rotation fluctuations and a wave/turbulence-driven model of the solar wind. *Astrophys. J.* **722**, 1495–1503.

HOLLWEG, J. V. & ISENBERG, P. A. 2007 Reflection of Alfvén waves in the corona and solar wind: an impulse function approach. *J. Geophys. Res.* **112**, 8102.

VAN DER HOLST, B., SOKOLOV, I. V., MENG, X., JIN, M., MANCHESTER IV, W. B., TÓTH, G. & GOMBOSI, T. I. 2014 Alfvén wave solar model (AWSoM): coronal heating. *Astrophys. J.* **782**, 81.

IROSHNIKOV, P. S. 1963 Turbulence of a conducting fluid in a strong magnetic field. *Astron. Zh.* **40**, 742.

KADOMTSEV, B. B. & POGUTSE, O. P. 1974 Nonlinear helical perturbations of a plasma in the tokamak. *Sov. J. Expl Theor. Phys.* **38**, 283.

KOPP, R. A. & HOLZER, T. E. 1976 Dynamics of coronal hole regions. I – Steady polytropic flows with multiple critical points. *Sol. Phys.* **49**, 43–56.

KRAICHNAN, R. H. 1965 Inertial-range spectrum of hydromagnetic turbulence. *Phys. Fluids* **8**, 1385.

MÜLLER, W. & GRAPPIN, R. 2005 Spectral energy dynamics in magnetohydrodynamic turbulence. *Phys. Rev. Lett.* **95** (11), 114502.

OFMAN, L. 2010 Wave modeling of the solar wind. *Living Rev. Sol. Phys.* **7** (1), 4.

PARKER, E. N. 1958 Dynamics of the interplanetary gas and magnetic fields. *Astrophys. J.* **128**, 664–676.

PARKER, E. N. 1965 Dynamical theory of the solar wind. *Space Sci. Rev.* **4**, 666.

PEREZ, J. C. & CHANDRAN, B. D. G. 2013 Direct numerical simulations of reflection-driven, reduced MHD turbulence from the Sun to the Alfven critical point. *Astrophys. J.* **776**, 124.

ROBERTS, P. H. & SOWARD, A. M. 1972 Stellar winds and breezes. *R. Soc. Lond. Proc.* A **328**, 185–215.

RUFFOLO, D. 1995 Effect of adiabatic deceleration on the focused transport of solar cosmic rays. *Astrophys. J.* **442**, 861.

SAGDEEV, R. Z. & GALEEV, A. A. 1969 *Nonlinear Plasma Theory*. W. A. Benjamin, Inc.

SHARMA, P., HAMMETT, G. W., QUATAERT, E. & STONE, J. M. 2006 Shearing box simulations of the MRI in a collisionless plasma. *Astrophys. J.* **637**, 952–967.

SHODA, M., SUZUKI, T. K., ASGARI-TARGHI, M. & YOKOYAMA, T. 2019 Three-dimensional simulation of the fast solar wind driven by compressible magnetohydrodynamic turbulence. *Astrophys. J.* **880** (1), L2.

SPANGLER, S. R. 1986 The evolution of nonlinear Alfven waves subject to growth and damping. *Phys. Fluids* **29**, 2535–2547.

STRAUSS, H. R. 1976 Nonlinear, three-dimensional magnetohydrodynamics of noncircular tokamaks. *Phys. Fluids* **19**, 134–140.

SUZUKI, T. K. 2006 Forecasting solar wind speeds. *Astrophys. J. Lett.* **640**, L75–L78.

SUZUKI, T. K. & INUTSUKA, S.-I. 2006 Solar winds driven by nonlinear low-frequency Alfvén waves from the photosphere: parametric study for fast/slow winds and disappearance of solar winds. *J. Geophys. Res.* **111**, 6101.

TENERANI, A., VELLI, M. & HELLINGER, P. 2017 The parametric instability of Alfvén waves: effects of temperature anisotropy. *Astrophys. J.* **851**, 99.

TU, C. & MARSCH, E. 1995 MHD structures, waves and turbulence in the solar wind: observations and theories. *Space Sci. Rev.* **73**, 1–210.

USMANOV, A. V., GOLDSTEIN, M. L. & MATTHAEUS, W. H. 2014 Three-fluid, three-dimensional magnetohydrodynamic solar wind model with eddy viscosity and turbulent resistivity. *Astrophys. J.* **788**, 43.

VELLI, M. 1993 On the propagation of ideal, linear Alfven waves in radially stratified stellar atmospheres and winds. *Astron. Astrophys*. **270**, 304–314.

VERDINI, A., GRAPPIN, R., PINTO, R. & VELLI, M. 2012 On the origin of the $1/f$ spectrum in the solar wind magnetic field. *Astrophys. J. Lett*. **750**, L33.

VERDINI, A. & VELLI, M. 2007 Alfvén waves and turbulence in the solar atmosphere and solar wind. *Astrophys. J*. **662**, 669–676.

VERDINI, A., VELLI, M., MATTHAEUS, W. H., OUGHTON, S. & DMITRUK, P. 2010 A turbulence-driven model for heating and acceleration of the fast wind in coronal holes. *Astrophys. J. Lett*. **708**, L116–L120.

WANG, Y. M. 1993 Flux-tube divergence, coronal heating, and the solar wind. *Astrophys. J. Lett*. **410**, L123.

WANG, Y., BOLDYREV, S. & PEREZ, J. C. 2011 Residual energy in magnetohydrodynamic turbulence. *Astrophys. J*. **740**, L36.